A Vaporization Model for Realistic Multi-Component Fuels

Shiyou Yang*, Youngchul Ra and Rolf D. Reitz
Engine Research Center, Department of Mechanical Engineering
University of Wisconsin-Madison
Madison, WI 53706-1609 USA

Abstract

A vaporization model for multi-component fuels is described. In the model a new approach named the discrete/continuous multi-component (DCMC) model, is used to describe the properties and composition of realistic multi-component gasoline fuels. With this approach gasoline is assumed to consist of five discrete families of hydrocarbons: n-paraffins, i-paraffins, naphthenes, aromatics, and olefins. Each family of hydrocarbons is composed of an infinite number of continuous components, which are modeled as a probability density function (PDF), and the mass fraction of each family of hydrocarbons (PDF), the mean and variance of each PDF are tracked. Compared with the discrete multi-component (DMC) model, which must model hundreds of components for gasoline, the DCMC model saves computer time. Compared with the continuous multi-component (CMC) model, the DCMC model has much higher accuracy. Unsteady vaporization of multi-component fuel can be described for both normal and flash-boiling evaporation conditions. An unsteady internal heat flux model and a model for the determination of the droplet surface temperature were formulated. An approximate solution to the quasi-steady energy equation was used to derive an explicit expression for the heat flux from the surrounding gas to the droplet-gas interface, with inter-diffusion of fuel vapor and the surrounding gas taken into account. The present vaporization models were implemented into a multi-dimensional CFD code and applied to calculate evaporation processes of single and multi-component fuel droplets.

*Corresponding author

Introduction

The evaporation of droplets of complex liquid mixtures, containing hundreds or thousands of components, is frequently encountered in engineering, particularly in combustors and engines burning commercial petroleum fuels. One treatment of this problem, which is more appropriate for mixtures with large numbers of components, is to describe the mixture properties using the methods of continuous thermodynamics (Tamim *et al*., [11]), in which composition is represented by a continuous probability density function with respect to an appropriate parameter, such as molecular weight. This approach is called the continuous multi-component (CMC) model. This enables a reduction of computational load without degrading the predictability of the complex behavior of the vaporization of multi-component fuels (Lippert, [5]).

However, when the CMC model is applied to combustion simulations, especially with detailed chemistry, describing the multi-component features of the fuel is inevitably limited, making it difficult to model the consumption of individual components appropriately. For this reason an alternative treatment of the evaporation of droplets of complex liquid mixtures is to describe the mixture properties using the discrete multi-component (DMC) model. The DMC approach tracks the individual components of the fuel during the evaporation process and allows coupling with the reaction kinetics of the individual fuel components. In the DMC model, the fuel is modeled as discrete fuel species, the characteristics of which are determined from fuel libraries (e.g., Torres *et al*. [12], Ra and Reitz [9]).

The disadvantage of the CMC model is that generally only a single PDF curve is used to represent the real fuel, which may be composed of multiple PDFs. Harstad *et al*. [4] have proposed a "double Γ PDF" CMC model in an attempt to describe more complex fuel distributions. However, it is difficult to generate this method to arbitrary fuels. In real fuels there are hundreds of discrete components. One disadvantage of the DMC model is that the computational cost is very high when it includes all the fuel components, because additional transport equations must be solved for each species in order to track the fuel composition and the vaporization behavior. Generally a real fuel is composed of several families of hydrocarbons. With this characteristic of a real fuel, the present paper proposes a DCMC (discrete/continuous multi-component) fuel model. The CMC approach is used for each group of hydrocarbons. Discrete PDFs (each PDF is a continuous multi-component family) represent the different families of hydrocarbons in the real fuel.

In this paper the theory of the new DCMC model is described briefly. The model was also implemented in a multi-dimensional CFD code (KIVA-3V Release 2) and was used to model the properties and composition of gasoline fuel. In this approach gasoline is assumed to be composed of five discrete families of hydrocarbons: n-paraffins, i-paraffins, naphthenes, aromatics, and olefins. Each family of hydrocarbons is composed of an infinite number of continuous components, which are modeled as a probability density function (PDF), and the mass fraction of each family of hydrocarbons (PDF), the mean and variance of each PDF are tracked.

Model Description

Vapor Phase Transport Equations

Suppose a flow field contains "*nsp*" species. The continuity equation for species "*m*" is:

$$\frac{\partial \rho_m}{\partial t} + \nabla \cdot (\rho_m \vec{\mathbf{v}}) = \nabla \cdot (\rho D \nabla y_m) + \frac{d}{dt}(\rho_m)^c + \frac{d}{dt}(\rho_m)^s , \quad (1)$$

where ρ_m is the mass density of species "*m*", ρ the total mass density, y_m the mass fraction of species "*m*", and $\vec{\mathbf{v}}$ the fluid velocity. We assume Fick's Law of diffusion with a single diffusion coefficient D. Superscript "*c*" means the source term is from chemistry, and "*s*" means the source term is from the spray. By summing Eq. (1) over all species we obtain the total fluid density equation

$$\frac{\partial \rho}{\partial t} + \nabla \cdot (\rho \vec{\mathbf{v}}) = \frac{d}{dt}(\rho)^s , \quad (2)$$

since mass is conserved in chemical reactions.

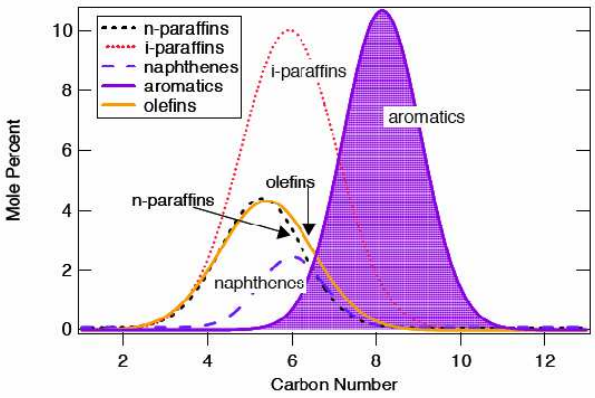

Figure 1. Chemical species distribution in gasoline (Farrell [2])

Figure 1 shows the chemical species distribution in a typical gasoline. As seen, gasoline mainly consists of five groups of hydrocarbons: n-paraffins, i-paraffins, naphthenes, aromatics, and olefins. In Figure 1 the species mole percent (probability density) of each group of

hydrocarbons as a function of carbon number is presented.

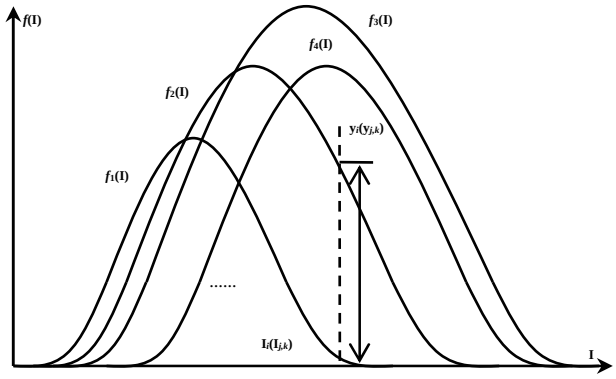

Figure 2. Each group of hydrocarbons is represented by a Γ-PDF

Now consider a general case: suppose the fuel vapor is either gasoline, or diesel, or ethanol, or blends of an arbitrary number of such these fuels; each group of hydrocarbons can be represented as a probability density function (PDF) of molecular weight $f_k(I)$, as shown in Figure 2. Any one species "*i*" with molecular weight "I_i" (which corresponds to a fixed carbon number) only comes from one group of hydrocarbons, e.g., "*k*". Suppose the total number of groups of hydrocarbons is K. The amount of species "*i*" is y_i (mass fraction), can be calculated by

$$y_i = y_{Fk} f_k(I_i)\Delta I_i , \tag{3}$$

where y_{Fk} is the mass fraction of the kth group of hydrocarbons in the gas phase, $f_k(I_i)$ the value of $f_k(I)$ at I_i, ΔI_i a small interval, and I the molecular weight. For the distribution function $f_k(I)$, we have

$$\int_0^\infty f_k(I)dI = 1 . \tag{4}$$

According to Eq. (1), the continuity equation for species "*i*" is:

$$\frac{\partial}{\partial t}(\rho y_i) + \nabla\cdot(\rho\vec{\mathbf{v}} y_i) = \nabla\cdot(\rho D\nabla y_i) + \frac{d}{dt}(\rho y_i)^c + \frac{d}{dt}(\rho y_i)^s . \tag{5}$$

Inserting Eq. (3) into Eq. (5),

$$\frac{\partial}{\partial t}(\rho y_{Fk} f_k(I_i)\Delta I_i) + \nabla\cdot(\rho\vec{\mathbf{v}} y_{Fk} f_k(I_i)\Delta I_i) = \nabla\cdot(\rho D\nabla(y_{Fk} f_k(I_i)\Delta I_i)) + \frac{d}{dt}(\rho y_{Fk} f_k(I_i)\Delta I_i)^c + \frac{d}{dt}(\rho y_{Fk} f_k(I_i)\Delta I_i)^s . \tag{6}$$

Summing over all species (from *j*=1 to n) in the kth group of hydrocarbons, gives

$$\frac{\partial}{\partial t}(\rho y_{Fk}) + \nabla\cdot(\rho\vec{\mathbf{v}} y_{Fk}) = \nabla\cdot(\rho D\nabla y_{Fk}) + \frac{d}{dt}(\rho y_{Fk})^c + \frac{d}{dt}(\rho y_{Fk})^s . \tag{7}$$

Equation (7) is the transport equation of the mass fraction y_{Fk} of the kth group of hydrocarbons.

Weighting Eq. (6) by $I_i^{\,m}$, then integrating, similarly we obtain the mth moment equation.

$$\frac{\partial}{\partial t}(\rho y_{Fk}\theta_k^{\,m}) + \nabla\cdot(\rho\vec{\mathbf{v}} y_{Fk}\theta_k^{\,m}) = \nabla\cdot(\rho D\nabla(y_{Fk}\theta_k^{\,m})) + \frac{d}{dt}(\rho y_{Fk}\theta_k^{\,m})^c + \frac{d}{dt}(\rho y_{Fk}\theta_k^{\,m})^s , \tag{8}$$

where we define $\theta_k^{\,m} = \int_0^\infty f_k(I) I^m dI$, which is the mth moment of the kth PDF.

If we use a two-parameter distribution function to track the variation of the kth PDF, we just need two additional transport equations in addition to the mass fraction transport equation. Substituting m=1 and m=2 into Eq. (8), we obtain the mean and second moment equations,

$$\frac{\partial}{\partial t}(\rho y_{Fk}\theta_k) + \nabla\cdot(\rho\vec{\mathbf{v}} y_{Fk}\theta_k) = \nabla\cdot(\rho D\nabla(y_{Fk}\theta_k)) + \frac{d}{dt}(\rho y_{Fk}\theta_k)^c + \frac{d}{dt}(\rho y_{Fk}\theta_k)^s , \tag{9}$$

$$\frac{\partial}{\partial t}(\rho y_{Fk}\psi_k) + \nabla\cdot(\rho\vec{\mathbf{v}} y_{Fk}\psi_k) = \nabla\cdot(\rho D\nabla(y_{Fk}\psi_k)) + \frac{d}{dt}(\rho y_{Fk}\psi_k)^c + \frac{d}{dt}(\rho y_{Fk}\psi_k)^s , \tag{10}$$

for the kth group of hydrocarbons.

The energy equation is

$$\overline{C}_P\frac{\partial}{\partial t}(\rho T) + \overline{C}_P\nabla\cdot(\rho\vec{\mathbf{v}} T) = \nabla\cdot\lambda\nabla T + [(a_c - C_{PA})\rho D\nabla y_F + b_c\rho D\nabla(\theta y_F)]\cdot\nabla T . \tag{11}$$

Liquid Phase Governing Equations

The form of the equation for composition change of the kth PDF species in the liquid phase is:

$$\frac{d\Theta_{kL}^{\,n}}{dt} = \frac{4\pi R^2\ddot{m}_k}{\rho_{kL}\frac{4\pi R^3}{3}}\frac{\Theta_{kL}^{\,1}}{\Theta_{kV}^{\,1}}(\Theta_{kL}^{\,n} - \Theta_{kV}^{\,n}) = \frac{3\ddot{m}_k}{\rho_{kL}R}\frac{\Theta_{kL}^{\,1}}{\Theta_{kV}^{\,1}}(\Theta_{kL}^{\,n} - \Theta_{kV}^{\,n}) , \tag{12}$$

Substituting n=1 and n=2 into Eq. (12), the governing equation for the change rate of the first and second moments of the kth PDF in the liquid phase is

$$\frac{d\Theta_{kL}}{dt} = \frac{3\ddot{m}_k}{\rho_{kL}R}\frac{\Theta_{kL}}{\Theta_{kV}}(\Theta_{kL} - \Theta_{kV}) , \tag{13}$$

$$\frac{d\Psi_{kL}}{dt} = \frac{3\dot{m}_k}{\rho_{kL} R}\frac{\Theta_{kL}}{\Theta_{kV}}(\Psi_{kL} - \Psi_{kV}) . \quad (14)$$

The vaporization mass flux $\dot{m}_k$ is closely coupled with the source terms $\frac{d}{dt}(\rho y_{Fk})^s$ in vapor phase governing equations. The calculation of $\dot{m}_k$ is given by Ra and Reitz [7].

The vapor phase source terms are derived by considering the molar flux at the droplet surface as

$$\Theta_k^{\ s} = Y_{F,R}\Theta_{kR} - \frac{1}{B}(Y_{Fk,\infty}\Theta_{k\infty} - Y_{Fk,R}\Theta_{kR})\frac{Y_{F,R}}{Y_{Fk,R}} , \quad (15)$$

$$\Psi_k^{\ s} = Y_{F,R}\Psi_{kR} - \frac{1}{B}\left(Y_{Fk,\infty}\Psi_{k\infty} - Y_{Fk,R}\Psi_{kR}\right)\frac{Y_{F,R}}{Y_{Fk,R}} . \quad (16)$$

Γ Distribution Function

The Γ distribution function adequately represents petroleum fractions and is expressed as

$$F_k(I) = \frac{(I-\gamma_k)^{\alpha_k - 1}}{\beta_k^{\ \alpha_k}\Gamma(\alpha_k)}\exp\left[-\left(\frac{I-\gamma_k}{\beta_k}\right)\right],$$

where α_k and β_k are two parameters controlling the shape of the k[th] PDF, and γ_k is the origin. The initial α_{kL}, β_{kL}, γ_{kL} describe the initial droplet composition. Thus,

$$\Theta_k = \int_0^\infty F_k(I) I dI = \alpha_k\beta_k + \gamma_k , \quad (17)$$

$$\sigma_k^{\ 2} = \int_0^\infty F_k(I)(I-\Theta_k)^2 dI = \alpha_k\beta_k^{\ 2} , \quad (18)$$

$$\Psi_k = \int_0^\infty F_k(I) I^2 dI = (\alpha_k\beta_k + \gamma_k)^2 + \alpha_k\beta_k^{\ 2} = \Theta_k^{\ 2} + \sigma_k^{\ 2} . \quad (19)$$

Vapor-Liquid Equilibrium

The vapor-liquid equilibrium (VLE) can be expressed in the form of Raoult's law:

$$Y_{FkV}F_{kV}(I_i)\Delta I_i P = Y_{FkL}F_{kL}(I_i)\Delta I_i P_k^{\ sat}(T, I_i) , \quad (20)$$

where $P_k^{\ sat}(T, I_i)$ indicates the saturated vapor pressure of species "*i*" at the droplet temperature T. Assuming a linear variation of boiling point temperature with composition,

$$T_{Bk}(I) = a_{Bk} + b_{Bk} I , \quad (21)$$

with a_{Bk} and b_{Bk} obtained from a regression of boiling point data for the k[th] PDF homologous family of components. Thus the saturated vapor pressure is expressed as

$$P_k^{\ sat}(T, I) = P_{atm} \cdot \exp\left[A_k(1 - B_k I)\right] , \quad (22)$$

where $A_k = \frac{s_{fg}}{\overline{R}}\left(1 - \frac{a_{Bk}}{T}\right)$, $B_k = \frac{b_{Bk}}{T - a_{Bk}}$. The molar fraction of the k[th] PDF at the droplet surface is

$$Y_{Fk,R} = Y_{FkL}\frac{P_{atm}}{P}\frac{\exp\left[A_k(1-\gamma_k B_k)\right]}{(1 + A_k B_k \beta_{kL})^{\alpha_{kL}}} . \quad (23)$$

The first and second moment of the distribution of the k[th] PDF can be obtained by weighting Eq. (20) with the distribution variable and integrating:

$$\Theta_{kV} = \gamma_k + \frac{\Theta_{kL} - \gamma_k}{1 + \frac{A_k B_k \sigma_{kL}^{\ 2}}{\Theta_{kL} - \gamma_k}}; \quad \sigma_{kV}^{\ 2} = \sigma_{kL}^{\ 2}\left[\frac{\Theta_{kV} - \gamma_k}{\Theta_{kL} - \gamma_k}\right]^2 . \quad (24)$$

Equation (24) shows the relations between the liquid phase and the vapor phase distribution parameters (at the droplet surface).

Determination of Surface Temperature

For more accurate predictions of the vaporization rate and heat flux, a surface temperature calculation model was incorporated by Ra and Reitz [8]. The surface temperature of the droplet is determined from a heat and mass transfer balance at the interface between the droplet and the surrounding gas. The rate of heat transfer balances with the required heat for vaporization at the surface following

$$L(T_s)\dot{m} = q_i + q_o , \quad (25)$$

where $L(T_s)$ is the latent heat of the fuel at the surface temperature T_s, $\dot{m}$ is the total vaporization mass flux, q_i is the heat transfer from inside the droplet, and q_o is the heat transfer from outside of the droplet. The detailed calculation of q_i and q_o in both normal evaporation and boiling cases is given by Ra and Reitz [7]. Neglecting the effect of radiation, the temporal change of the droplet temperature is given as

$$\frac{dT_d}{dt} = \frac{Ah_{i,eff}(T_s - T_d)}{\rho c_v V} \text{ for normal evaporation, } (26)$$

$$\frac{dT_d}{dt} = \frac{A\alpha(T_b - T_d)}{\rho c_v V} \text{ for flash boiling, } (27)$$

where ρ is the droplet density, A and V are the droplet surface area and volume, respectively, c_v is the specific heat at constant volume of the liquid phase at the droplet temperature, $h_{i,eff}$ and α are the effective heat transfer coefficients for the normal evaporation and boiling cases, respectively, and T_b is the boiling temperature. Eqs. (26) and (27) are solved implicitly in the computer code.

Code Development

The DCMC model described above was implemented into the ERC-KIVA3V-DMC code. In the implementation each fuel component in the DMC model was extended as a PDF. The mass fraction, mean and the second moment of each PDF are tracked in the calculation. At the beginning of calculation, the initial mass fraction, α, β, γ of each PDF are read from an input file.

Results and Analysis

Results from DMC model

Since the DCMC model is based on the DMC model, the experimental results were compared with those from the DMC model. The DMC evaporation model was compared with experimental results of Gokalp *et al*. [3] and Nomura *et al*. [6] for single component droplet evaporation. Figure 3 shows comparisons of the drop size history for n-heptane droplets under stationary, micro-gravity conditions. The experimental data are from Nomura *et al*. [6]. The ambient pressure is 1 bar, and the initial drop diameter is 0.6 mm. It is seen that the DMC model predictions are in good agreement with the experimental measurements for various ambient temperatures.

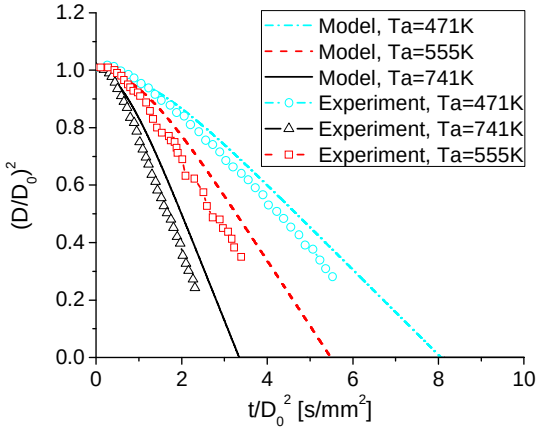

Figure 3. Comparison between DMC simulation and available experimental data (Ra and Reitz [9])

Evaporation of a single gasoline drop was also simulated using the DMC model (Ra and Reitz, [9]). In order to model the composition of typical gasoline fuel, seven hydrocarbon species were considered (Ra and Reitz, [9]). The distillation curves of the modeled fuel are shown in Figure 4. The measurement data are from Smith and Bruno [10]. The calculation conditions in Figure 4 are as follows: D_0=100 μm, T_{d0}=313 K, P_0=1 bar, T_0=500 K. It is seen that the predicted distillation characteristics of the fuel are in good agreement with the measured data.

The evaporation of a single diesel drop was also simulated using the DMC model. In order to model the composition of a typical diesel fuel, six hydrocarbon species were considered (Ra and Reitz, [9]). The distillation curves of the modeled diesel fuel are shown in Figure 5. The measurement data are from Butts [1]. The calculation conditions in Figure 5 are as follows: D_0=100 μm, T_{d0}=360 K, P_0=1 bar, T_0=500 K. It is seen that the predicted distillation characteristics of the fuel are in excellent agreement with the measured data. Since the volatility of diesel fuel components is much lower than those of gasoline, the distillation temperatures are much higher than those of gasoline.

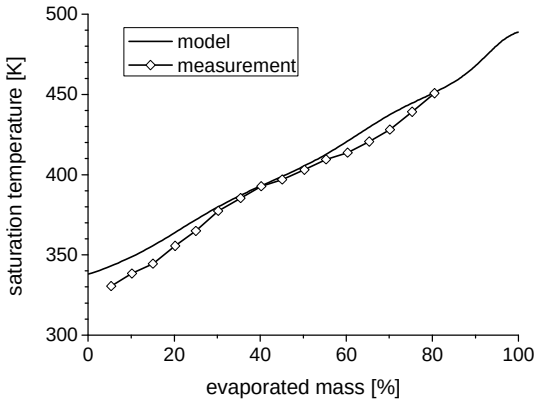

Figure 4. Comparison of distillation curves of gasoline fuel between modeled and measured data

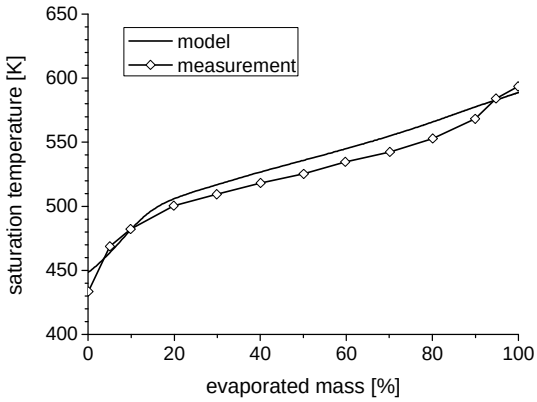

Figure 5. Comparison of distillation curves of diesel fuel between modeled and measured data

Comparison between DCMC Using Delta Function PDFs and DMC

The DCMC code is tested with seven delta functions (narrow PDFs) for gasoline fuel. The results are compared with the above results from the DMC code using seven discrete components for gasoline fuel. Fig-

ure 6(a) compares the mass and surface area histories between the DCMC and DMC. Figure 6(b) compares the droplet interior temperature, surface temperature, and saturation temperature while Figure 6(c) compares the droplet surface mass fraction, and Figure 6(d) compares the droplet interior mass fraction. The simulation conditions are the same as in Figure 4. The match between DCMC and DMC is reasonably good. In the early stage of evaporation DCMC under-predicts DMC results, and in the late stage DCMC over-predicts DMC results. The difference is due to the fact that some physical properties calculated from the CMC correlation do not

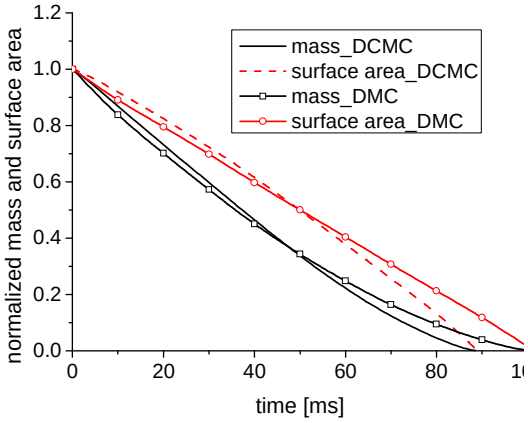

(a)

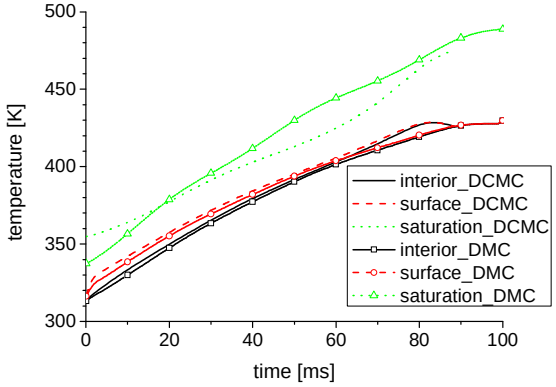

(b)

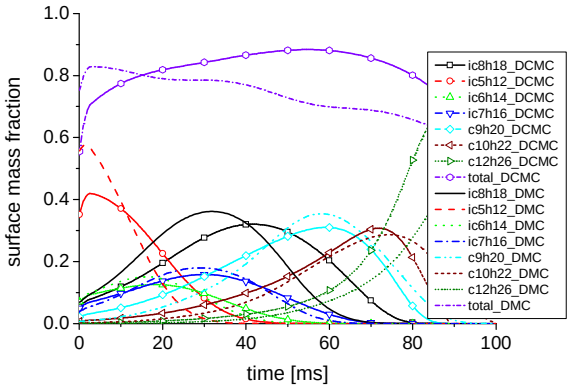

(c)

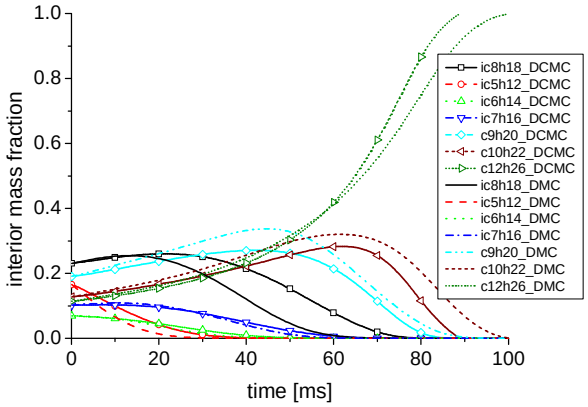

(d)

Figure 6. Comparison between DCMC using delta functions and DMC

exactly match those from the DMC libraries. For example, the enthalpy of vaporization from the CMC correlation is higher in the early stage, while this property from CMC correlation is lower in the late stage.

Comparison between a Single Broad PDF and a Single Component Using DCMC

The DCMC code was also tested with a single broad PDF for gasoline fuel. The results were compared with those from representing gasoline fuel as a single component. The comparison is shown in Figure 7. Figure 7(a) compares the mass, the surface area and the mean of the fuel, while Figure 7(b) compares the droplet interior temperature, surface temperature, and saturation temperature. The simulation conditions were the same as in Figure 4. The parameters for the single PDF were: α=5.7, β=15.0, γ=0.0. Correspondingly the parameters for the single component were: α=100.0, β=0.1, γ=104.2.

Because the highly volatile light-end components in the broad PDF gasoline composition evaporate preferentially, both the droplet size and mass decrease rapidly in the initial stage, and the mean molecular weight of the composition increases steadily. However, compared with single component, the evaporation rate of broad PDF gasoline slows down during the later stages. The mean molecular weight of the single component remains unchanged. Figure 7(b) shows a characteristic of multi-component fuel vaporization: the broad PDF gasoline droplets do not reach an equilibrium temperature (both interior and surface temperatures) as in the case of the single-component case, because the composition of the broad PDF is continuously changing as the more volatile components are vaporized. Also it is seen that the saturation temperature of the broad PDF case is continuously increasing, while the saturation temperature of the single-component case remains unchanged.

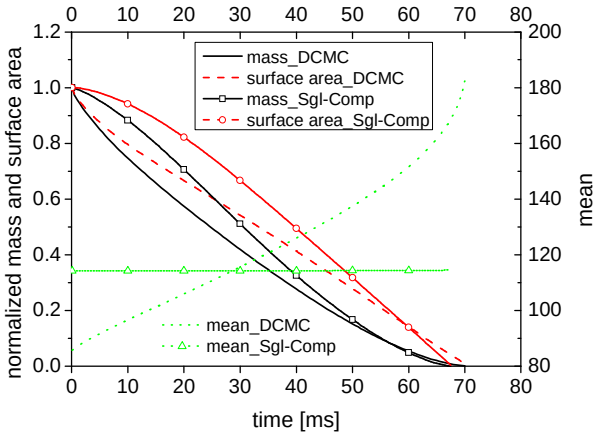

(a)

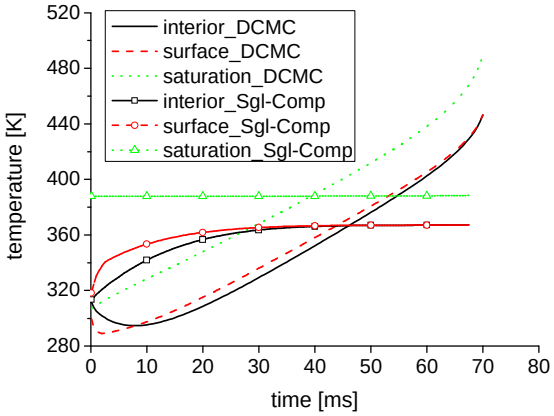

(b)

Figure 7. Comparison between a single broad PDF and a single component using DCMC

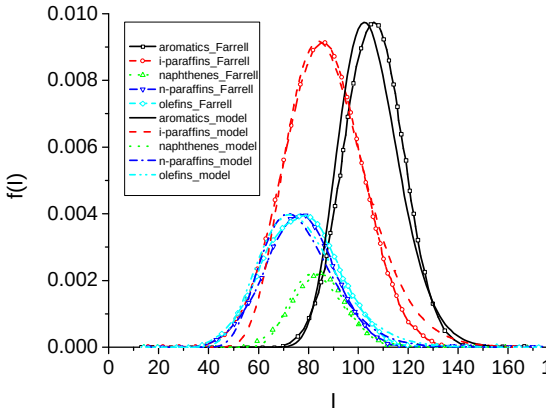

(a) Initial distributions

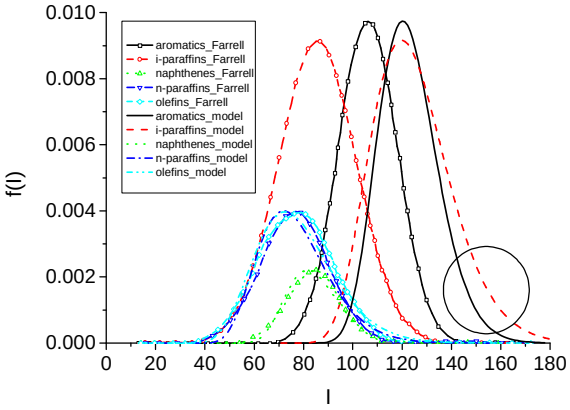

(b) Model predicted distributions at 85 ms

Figure 8. PDF curves from model and Farrell

Simulation of Single Gasoline Droplet by Using DCMC

A single gasoline droplet was simulated using the present DCMC code. As described above the gasoline is assumed to consist of five families of hydrocarbons: n-paraffins, iso-paraffins, olefins, naphthenes, and aromatics, as shown in Figure 1. The mass fraction and the composition parameters α, β, γ of each family of hydrocarbons are shown in Table 1. The simulated conditions are the same as in Figure 4. Figure 8(a) shows each PDF curve used in the simulation together with the PDF curve from Farrell [2]. It is seen that the PDFs represent gasoline well.

Table 1. Mass fraction and composition of each PDF

	mass fraction	α	β	γ
n-paraffins	0.1378	8.4	5.0	35.0
iso-paraffins	0.3591	11.0	4.9	35.0
olefins	0.1532	10.7	4.9	25.0
naphthenes	0.0584	13.2	3.0	45.0
aromatics	0.2915	19.0	2.8	52.0

Figure 9 shows the simulated results. Figure 9(a) shows drop mass and surface area, Figure 9(b) shows drop interior, surface and saturation temperatures, Figure 9(c) shows drop surface mass fraction, Figure 9(d) shows drop interior mass fraction, and Figure 9(e) shows the mean of each PDF. The drop size varies in the manner of the well-known D^2-law, as shown in Figure 9(a). Figure 9(b) shows that due to preferential vaporization of the more volatile light-end components in each family and preferential vaporization of light-end family itself, the composition of the droplet changes continuously, saturation temperature increases gradually, and thus gasoline droplet does not reach an equilibrium condition. The droplet surface temperature is a little higher than the interior temperature, which indicates that the droplet is heated up. During the drop life time the total mass fraction of fuel at the drop surface is less than unity, which means that vaporization occurs in the normal evaporation regime, as shown in Figure 9(c). Since in the current model n-paraffins, iso-paraffins, naphthenes, olefins are light-end families, they evaporate fast, compared with the heavy-end family aromatics, the droplet interior mass fractions of n-paraffins,

iso-paraffins, naphthenes, olefins decrease continuously, and the droplet interior mass fraction of aromatics increases continuously, as shown in Figure 9(d). Due to preferential vaporization of the more volatile light-end components in each family, heavier components remain in each family and each family changes to a narrower PDF, and the mean of each PDF increases continuously, as shown in Figure 9(e). However, it is interesting that around 85 ms, the droplet interior mass fraction of aromatics decreases while that of the iso-paraffins increases.

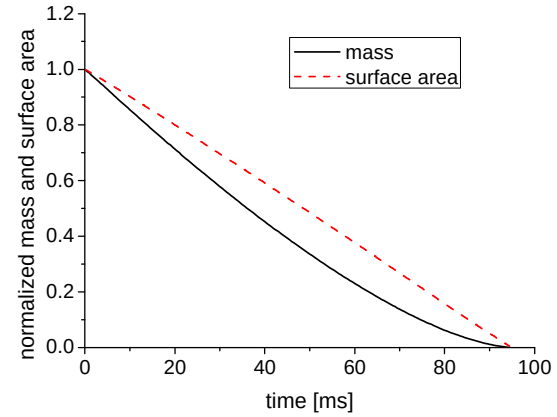

(a)

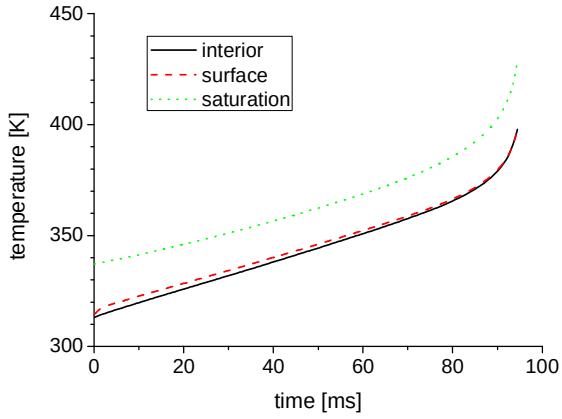

(b)

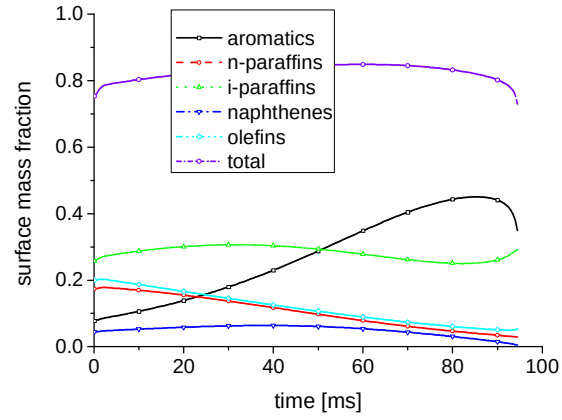

(c)

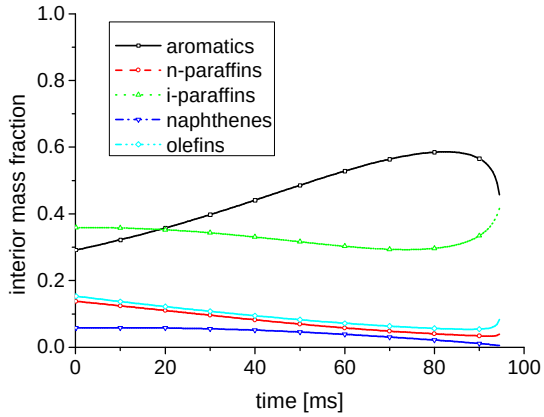

(d)

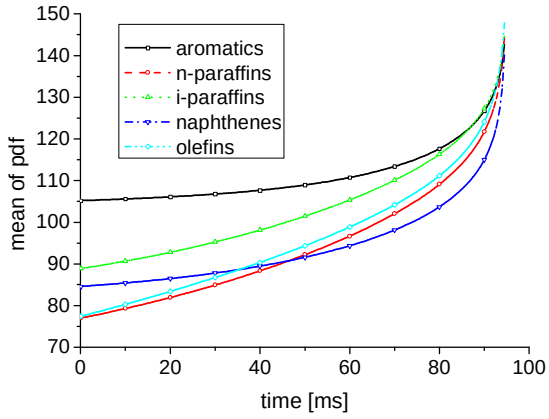

(e)

Figure 9. Simulated results of a single gasoline drop using the DCMC model

This phenomena was not found in the results from the DMC model, which are not presented in this paper due to the limitation of length. This interesting difference can be explained as follows: Initially, compared with the aromatics the iso-paraffins is light-end family, as can be seen in Figure 8(a). The iso-paraffins evaporates fast, and thus its PDF curve moves to the right at a higher speed, relative to the aromatics. Around 85 ms the mean of iso-paraffins is the same as that of aromatics. At this time the two PDF curves of iso-paraffins and aromatics are located in the position shown in Figure 8(b). Because the variance of iso-paraffins is wider than that of aromatics, there are more heavy components in the iso-paraffins family. After this time, the PDF curve of iso-paraffins is located slightly to the right of that of aromatics (indicated by the circle). This means that iso-paraffins will be the heavy-end family, and the evaporation rate slows down.

Conclusions

In this paper a DCMC (discrete/continuous multi-component) fuel vaporization model was developed, and was implemented into a 3-D CFD code. The CMC approach was used to describe separate groups of hydrocarbons. Multiple discrete PDFs (each PDF is a continuous multi-component mixture) represent the different families of hydrocarbons in the real fuel. Results from seven delta functions (narrow PDFs) for a gasoline fuel surrogate using the DCMC code and results from seven discrete components for gasoline fuel using the DMC code, matched well. Also, results from a single broad PDF representing gasoline using the DCMC code were reasonable, compared with results representing gasoline fuel as a single component. Finally, the present DCMC code was used to model vaporization of realistic gasoline fuel. Using five discrete families of hydrocarbons, each of which was modeled as a PDF distribution, DCMC model could successfully distinct the evaporation of components in different families that have similar molecular weights, and the mass fraction of each family of hydrocarbons (PDF), the mean and variance of each PDF could be tracked. Some new features of the vaporization of realistic fuels were revealed using the DCMC model that depends on the details of the fuel distributions. For example, toward the end of the droplet lifetime, initially lighter components could outlive the last remaining heavy components.

Acknowledgements

This work was supported by Ford Research and Advanced Engineering who is thanked for providing useful comments.

References

1. Butts, R. (2008). Investigation of the Effects of Fuel Properties on Low Temperature Combustion in a Highly Dilute Light Duty Diesel Engine. M. S. Thesis, University of Wisconsin-Madison.
2. Farrell. (2007). Private Communication, University of Wisconsin-Madison.
3. Gokalp, I., Chauveau, C., Berrekam, H., Ramos-Arroyo, N. A. (1994). Vaporization of Miscible Binary Fuel Droplets Under Laminar and Turbulent Convective Conditions. Atomization and Sprays 4, 661-676.
4. Harstad, K. G., Clercq, P. C. Le, and Bellan, J. (2003). Statistical Model of Multicomponent-Fuel Drop Evaporation for Many-Drop Flow Simulations. AIAA Journal, 41, No. 10, 1858-1874.
5. Lippert, A. M. (1999). Modeling of Multi-Component Fuels with Application to Sprays and Simulation of Diesel Engine Cold Start. Ph.D. Thesis, University of Wisconsin-Madison.
6. Nomura, H., Ujiie, Y., Rath, H. J., Sato, J., and Kono, M. (1996). Experimental Study on High-Pressure Droplet Evaporation Using Microgravity Conditions. Proc. Combust. Inst. 26, 1267-1273.
7. Ra, Y. and Reitz, R. D. (2003). The Application of a Multi-Component Droplet Vaporization Model to Gasoline Direct Injection Engines. Int. J. Engine Res., 4(3), 193-218.
8. Ra, Y. and Reitz, R. D. (2004). A Model for Droplet Vaporization for Use in Gasoline and HCCI Engine Applications. J. Eng. Gas Turb. Power, 126, 422-428.
9. Ra, Y. and Reitz, R. D. (2009). A Vaporization Model for Discrete Multi-Component Fuel Sprays. International Journal of Multiphase Flow, 35, 101-117.
10. Smith, B. L., Bruno, T. J. (2007). Improvements in the measurement of distillation curves. 3. Application to Gasoline and Gasoline + Methanol Mixtures. Int. Eng. Chem. Res. 46, 297-309.
11. Tamim, J. and Hallett, W. L. H. (1995). Continuous Thermodynamics Model for Multi-Component Vaporization. Chem. Engr Sci., 50(18), 2933-2942.
12. Torres, D. J., O'Rourke, P. J., and Amsden, A. A. (2003). A Discrete Multi-Component Fuel Model. Atomization and Sprays, Vol. 13, pp. 131-172.